Switching Transient-Based Junction Temperature Estimation of SiC MOSFETs With Aging Compensation

Masoud Farhadi, *Member, IEEE*, Rahman Sajadi, Bhanu Teja Vankayalapati, *Member, IEEE*, and Bilal Akin, *Fellow, IEEE*

***Abstract*—This article puts forward a novel online method to measure the junction temperature (T_j) of silicon carbide (SiC) MOSFETs. In this method, the voltage spikes in the common source stray inductance are captured to obtain the turn-ON and turn-OFF switching transients of SiC MOSFETs. The switching transients contain useful information pertaining to the temperature and are used to extract the junction temperature. By measuring both turn-ON and turn-OFF switching transients, the technique effectively addresses the impact of aging on the online junction temperature measurement procedure. The proposed method enables the measurement of junction temperature without high-bandwidth current sensors. In order to improve precision, this approach converts the measured voltage spikes into digital signals with specific pulse width, which can be measured by high-resolution capture module in the microcontroller with an error of less than 1 °C. Importantly, the proposed circuit has minimal impact on the normal operation of the converter and can be integrated into the gate driver integrated circuits (ICs). The effectiveness of this method is validated through experiments conducted on a double-pulse test setup and buck converter. The results confirm the practicality and viability of this approach.**

***Index Terms*—Aging, gate-oxide degradation, junction temperature, reliability, silicon carbide (SiC), switching transient, temperature-sensitive electrical parameter (TSEP).**

I. Introduction

Silicon carbide (SiC) MOSFETs have several advantages over traditional silicon-based MOSFETs, including higher switching speed, higher temperature capability, and lower losses, which make them an attractive choice for a wide range of power electronics applications [1], [2], [3]. Online junction temperature measurement is of particular importance for these devices due to several reasons. First, online junction temperature measurement can prevent excessive temperature by providing real-time feedback on the device's temperature, as SiC MOSFETs are meant to operate at high temperatures. Second, aging indicators, including threshold voltage and on-state resistance, exhibit temperature-dependent properties. As a result, precise temperature measurement is necessary to monitor these precursors for possible issues. In addition, temperature monitoring can yield vital information for creating more efficient heat dissipation systems, allowing for better power management and longer device lifetimes.

Different junction temperature measurement methods can be classified into three categories, which comprise on-chip temperature sensors [4], [5], estimation based on thermal impedance [6], [7], and methods that rely on temperature-sensitive electrical parameters (TSEPs) [8], [9], [10], [11]. Among these solutions, TSEPs are frequently employed solutions for junction temperature measurement due to their cost-effectiveness, noninvasiveness, and ease of integration into existing systems. They can provide an indirect indication of the junction temperature without necessitating any device or package modifications.

Over the past several years, different TSEPs have been reported in the literature for junction temperature measurement. The measurement of MOSFET junction temperature using the on-resistance ($R_{\mathrm{DS,ON}}$) is discussed in [12], [13], and [14]. The temperature dependence of $R_{\mathrm{DS,ON}}$ can be attributed to the temperature dependency of two components: channel resistance and drift region resistance. Channel resistance typically decreases with increasing temperature owing to an increase in channel mobility (μ_{ch}), whereas drift region resistance tends to increase due to lattice vibration [15]. Consequently, $R_{\mathrm{DS,ON}}$ can exhibit either a positive or negative temperature coefficient, depending on the interplay between these two competing resistances. Based on the vendor datasheets, the on-resistance of MOSFETs tends to increase nonlinearly with temperature, and hence, it is difficult to use it as a reliable indicator of junction temperature. In addition, the on-resistance of SiC MOSFETs is typically in the range of a few milliohms, therefore, measuring small changes in on-resistance is a bit challenging. In [16], the threshold voltage (V_{th}) has been suggested as a suitable parameter to measure junction temperature, given its strong sensitivity and linear correlation with

Manuscript received 2 November 2023; revised 14 April 2024; accepted 17 May 2024. Date of publication 27 May 2024; date of current version 4 September 2024. This work was supported by the Texas Instruments and Semiconductor Research Corporation (SRC)/Texas Analog Center of Excellence (TxACE) under Grant 2810.054. Recommended for publication by Associate Editor H. Wang. *(Corresponding author: Bilal Akin.)*

Masoud Farhadi and Bhanu Teja Vankayalapati are with the Texas Instruments, Dallas, TX 75243 USA (e-mail: m-farhadi@ti.com; b-vankayalapati@ti.com).

Rahman Sajadi and Bilal Akin are with the Department of Electrical and Computer Engineering, University of Texas at Dallas, Richardson, TX 75080 USA (e-mail: abdolrahman.sajadi@utdallas.edu; bilal.akin@utdallas.edu).

Color versions of one or more figures in this article are available at https://doi.org/10.1109/TPEL.2024.3404873.

Digital Object Identifier 10.1109/TPEL.2024.3404873

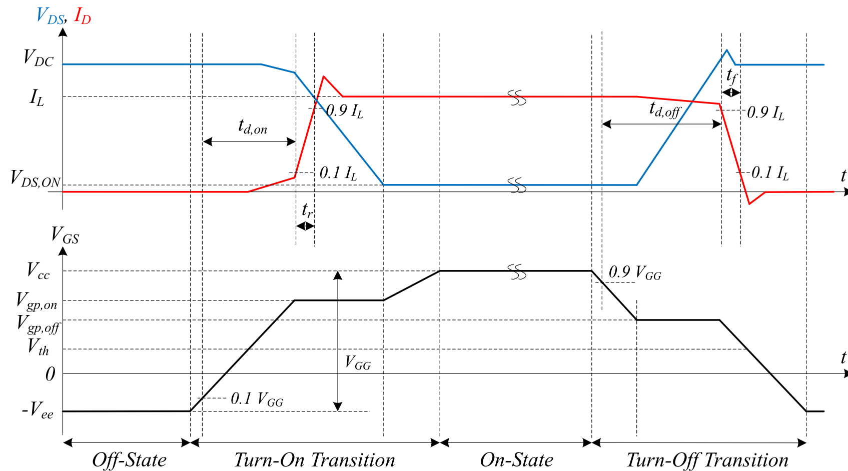

Fig. 1. Illustration of idealized turn-ON and turn-OFF switching transient for SiC MOSFET.

temperature. However, measuring V_{th} during converter operation requires high-resolution analog-to-digital converter (ADC) and noise cancellation techniques, which limit its practicability as a solution. The peak gate current observed during the turn-ON delay period has also been demonstrated as an effective TSEP to measure the junction temperature [17], [18]. As discussed in [19], this approach imposes strict requirements on device manufacturing and is limited to certain SiC MOSFETs with controlled gate designs. The turn-ON and turn-OFF delay times have been identified as promising TSEPs to measure the junction temperature. Recently, these TPEPS have been adopted for real-time junction temperature measurement with decent linearity [20], [21], [22]. By utilizing intelligent gate drivers and relatively high gate resistance, the sensitivity of these TSEPs can be further improved. The linearity and sensitivity of the body diode voltage can also be used for the same purpose at low-current injection, as reported in [23]. Achieving low-current injection can be done in reliability test setups but it is not straightforward for converter operations. In [24], the short-circuit current exhibits a favorable linear relationship with the junction temperature and can be employed as a TSEP. However, caution should be exercised as self-heating effects may impact the accuracy of the measurement and result in increased package aging. As a TSEP, turn-ON switching transient is used in [25], and the oscilloscope measurements show sufficient sensitivity and linearity. However, the practical implementation of this method poses a challenge due to the high-switching frequency of SiC MOSFETs, and a thorough examination of its online implementation has yet to be discussed in previous studies.

In the aforementioned studies, it was presumed that the temperature dependency of the TSEPs does not change throughout the lifetime [26], [27], [28], [29]. However, the deterioration of the gate oxide and package can greatly impact TSEPs and override this assumption. Therefore, the integration of an aging compensation scheme into TSEP-based temperature measurement circuits is crucial.

In response to the challenges outlined above, this article presents a practical solution for online junction temperature measurement based on switching transient that considers the entire signal chain. Specifically, this article utilizes the rise time (t_r) and fall time (t_f) of SiC MOSFETs as temperature-dependent parameters. It is shown that these parameters exhibit significant sensitivity to temperature in Section II. In Section III, a new circuit design is proposed for online measurement of switching transients, eliminating the requirement for high-bandwidth current sensors. The proposed circuit has minimal impact on the converter's normal operation and can be integrated into the gate driver integrated circuit (IC). Furthermore, Section IV investigates the aging dependency of these parameters by conducting an active channel gate bias (ACGB) test. By measuring the switching transient time during both turn-ON and turn-OFF, the effects of temperature and aging are effectively separated. Finally, Section V concludes this article.

II. Temperature Effect on the Turn-ON and Turn-OFF Switching Transients

In this section, a comprehensive explanation of the switching transients of SiC MOSFET is provided. In addition, the influence of temperature on these switching transients is thoroughly examined. More specifically, the analysis focuses on the correlation between the variation of di_D/dt and related parameters, such as rise time and fall time, with respect to junction temperature. In the following sections, this analysis of the temperature dependency of rise time and fall time is applied to construct a composite TSEP with aging compensation. To be more precise, it utilizes the portions of the t_r and t_f during which the voltage drop across the common source exhibits a linear alteration. This approach is employed to facilitate a more convenient and accurate measurement of the junction temperature.

Fig. 1 shows the idealized turn-ON and turn-OFF switching transients for SiC MOSFET. During the turn-ON switching process, the gate–source voltage (V_{GS}) of the SiC MOSFET gradually increases from the negative gate supply voltage ($-V_{\mathrm{ee}}$) to the positive gate supply voltage (V_{cc}). As V_{GS} increases, the depletion layer starts to shrink, resulting in the formation of a

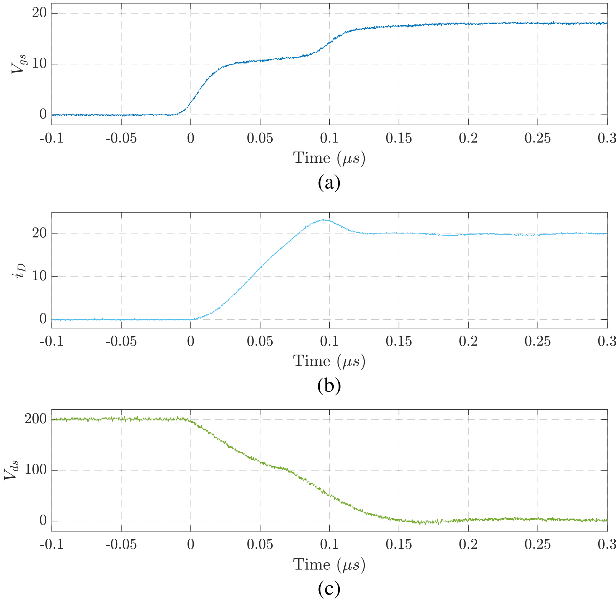

Fig. 2. Illustration of the turn-ON switching transient ($R_g = 5\ \Omega$). (a) Gate–source voltage. (b) Drain current. (c) Drain–source voltage.

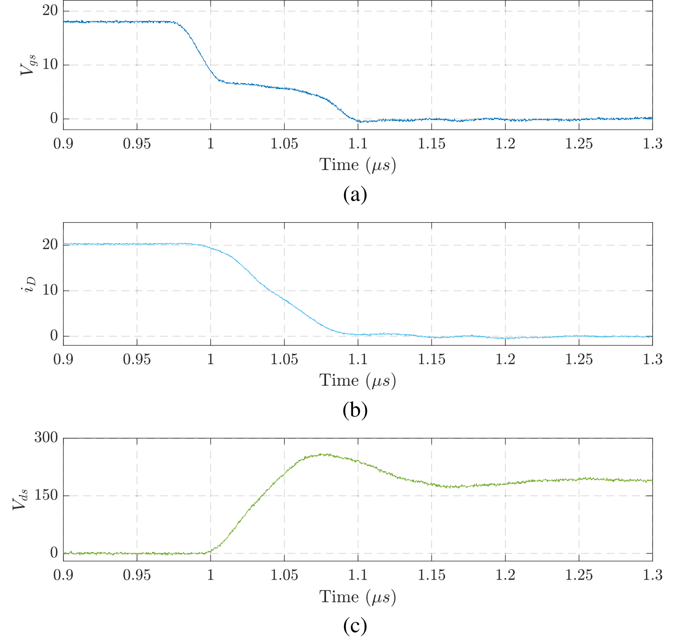

Fig. 3. Illustration of the turn-OFF switching transient ($R_g = 5\ \Omega$). (a) Gate–source voltage. (b) Drain current. (c) Drain–source voltage.

conducting channel between the source and drain. First, the input capacitance is charged until V_{GS} reaches the threshold voltage. During this turn-ON delay stage ($t_{d,\mathrm{on}}$), the drain current (I_D), and drain–source voltage (V_{DS}) remain unchanged. Once V_{GS} reaches V_{th}, the MOSFET is turned-ON and I_D will start to decrease. The gate–source voltage continues to rise until it reaches the Miller plateau voltage, at which point the reverse recovery current of the freewheeling diode starts to decrease from its peak value to zero, and V_{DS} gradually decreases until it reaches the on-state voltage ($V_{\mathrm{DS,ON}}$). Here, the Miller capacitance is charged, and the MOSFET is kept in the saturation region. Finally, as V_{GS} reaches to V_{cc}, the MOSFET is fully turned-ON with V_{DS} and I_D at the load current which is shown in Fig. 2. In the turn-OFF phase of MOSFET (see Fig. 3), V_{GS} is lowered from V_{cc} to $-V_{\mathrm{ee}}$, which leads to the widening of the depletion layer and shrinking of the conducting channel. However, due to the presence of energy stored in the inductive load, the drain current cannot instantly drop to zero, leading to a momentary increase in the voltage across the MOSFET and causing a reverse recovery current to flow through the freewheeling diode. This reverse recovery current may cause a brief overshoot of the drain current before dropping to zero. Moreover, the circuit's parasitic capacitances can also contribute to the voltage across the MOSFET oscillating around $V_{\mathrm{DS,ON}}$ as the MOSFET switches from the on-state to the off-state.

A. di_D/dt Temperature Dependency

di_D/dt directly influences the t_r and t_f of the drain current. t_r refers to the time it takes for the channel current to change from a low level (10%) to a high level (90%), whereas fall time represents the transition from a high level to a low level. A higher di_D/dt value corresponds to quicker rise and fall times, indicating a rapid transition between high- and low-current states. Conversely, a lower di_D/dt value indicates slower rise and fall times, signifying a more gradual transition.

Given that the MOSFET is in the saturation region during switching transients, the drain current at the t_r and t_f time instants can be represented as [30]

$$i_D = \frac{\beta}{2}\left(V_{\mathrm{gs}} - V_{\mathrm{th}}\right)^2\left(1 + \lambda\left(V_{\mathrm{gs}} - V_{\mathrm{th}}\right)\right) \quad (1)$$

$$\beta = \frac{W\mu_0 C_{\mathrm{OX}}}{L}. \quad (2)$$

Here, the channel width is represented by W, the channel length is denoted by L, λ signifies the channel length modulation parameter, μ_0 is the effective carrier mobility of the channel, and C_{OX} refers to the gate oxide capacitance of SiC MOSFET. The rate of change of the drain current with respect to time can be expressed as

$$\frac{di_D}{dt} = \frac{\beta}{2}\left(V_{\mathrm{gs}} - V_{\mathrm{th}}\right)\left(2 + 3\lambda\left(V_{\mathrm{gs}} - V_{\mathrm{th}}\right)\right)\frac{\mathrm{d}V_{\mathrm{gs}}}{\mathrm{d}t}. \quad (3)$$

The following expressions can be used to attain V_{gs} values for turn-ON and turn-OFF transients

$$V_{\mathrm{gs,on}} = V_{\mathrm{cc}}\left(1 - \mathrm{e}^{-(t/R_{\mathrm{g}}C_{\mathrm{iss}})}\right) \quad (4)$$

$$V_{\mathrm{gs,off}} = V_{\mathrm{cc}}\mathrm{e}^{-(t/R_{\mathrm{g}}C_{\mathrm{iss}})}. \quad (5)$$

The turn-ON and turn-OFF di_D/dt values can be obtained by differentiating (4) and (5) with respect to time and substituting the results into (3)

$$\frac{di_{D,\mathrm{on}}}{dt} = \frac{\beta V_{\mathrm{cc}}}{2R_{\mathrm{g}}C_{\mathrm{iss}}}A(2 + 3\lambda A)\mathrm{e}^{-(t/R_{\mathrm{g}}C_{\mathrm{iss}})} \quad (6)$$

$$\frac{di_{D,\mathrm{off}}}{dt} = -\frac{\beta V_{\mathrm{cc}}}{2R_{\mathrm{g}}C_{\mathrm{iss}}}B(2 + 3\lambda B)\mathrm{e}^{-(t/R_{\mathrm{g}}C_{\mathrm{iss}})} \quad (7)$$

where

$$A = V_{\text{cc}}\left(1 - \mathrm{e}^{-(t/R_{\text{g}}C_{\text{iss}})}\right) - V_{\text{th}} \tag{8}$$

$$B = V_{\text{cc}}\mathrm{e}^{-(t/R_{\text{g}}C_{\text{iss}})} - V_{\text{th}}. \tag{9}$$

To evaluate how temperature affects the current commutation rate, the derivative of (6) and (7) with respect to temperature can be calculated with respect to temperature. Two parameters that are affected by temperature in (6) and (7) are the threshold voltage and β. The value of β is influenced by the effective mobility of the carriers present in the channel. β in SiC MOSFETs demonstrates a nonlinear relationship with temperature. At lower temperatures, β increases, exhibiting a positive temperature coefficient. However, as the temperature increases further, β starts to decrease and demonstrates a negative temperature coefficient. This is because the influence of lattice scattering dominates in this temperature range. Within the practical operational temperature range of 30–175 °C, it can be assumed that β remains relatively constant and maintains a positive value [31], [32]. As a result, it can be assumed that the effect of β on the temperature dependence of the current commutation rate is negligible for SiC MOSFETs. In (6) and (7), the input capacitance (C_{iss}) is highly dependent on the voltage across the drain and source terminals. In practical scenarios, this voltage is equal to the dc-bus voltage, which remains constant.

The threshold voltage is the minimum voltage required at the gate terminal to turn-ON the device and establish a conducting channel between the source and drain terminals. It is challenging to calculate the temperature dependence of the threshold voltage theoretically because it is a function of several parameters, and there is limited information available from manufacturers regarding the fabrication parameters. However, this temperature dependency can be achieved through experimental results. As reported experimentally in [33], threshold voltage shows a negative temperature coefficient. Temperature dependency of di_D/dt during turn-ON and turn-OFF can be expressed as

$$\frac{d^2 I_{\text{D,on}}}{dtdT} = -\frac{\beta V_{\text{cc}}}{2R_{\text{g}}C_{\text{iss}}}(2 + 6\lambda A)\mathrm{e}^{-(t/R_{\text{g}}C_{\text{iss}})}\frac{dV_{\text{th}}}{dT} \tag{10}$$

$$\frac{d^2 I_{\text{D,off}}}{dtdT} = \frac{\beta V_{\text{cc}}}{2R_{\text{g}}C_{\text{iss}}}(2 + 6\lambda B)\mathrm{e}^{-(t/R_{\text{g}}C_{\text{iss}})}\frac{dV_{\text{th}}}{dT} \tag{11}$$

where "T" represents temperature. The temperature dependence of di_D/dt during turn-ON and turn-OFF in SiC MOSFETs can be deducted by considering the positive value of beta and negative value of dV_{th}/dT. Specifically, the temperature dependency of di_D/dt for SiC MOSFETs during turn-ON is positive, while during turn-OFF, it is negative. Consequently, the temperature dependence of t_r and t_f for SiC MOSFETs is found to be negative and positive, respectively. However, for silicon MOSFETs, the rise time is either independent of temperature or increases as the temperature increases [34]. The difference in temperature dependency between SiC MOSFETs and silicon MOSFETs can be attributed to $d\beta/dT$, which has a very low value in SiC MOSFETs, but it is negative in silicon MOSFETs [31].

Fig. 4 illustrates the parasitic capacitances within SiC MOSFETs. These include: gate-to-source capacitance (C_{gs}), which is in parallel with the series connection of gate-to-drain capacitance (C_{gd}) and drain-to-source capacitance (C_{ds}). The input capacitance (C_{iss}) can be expressed as

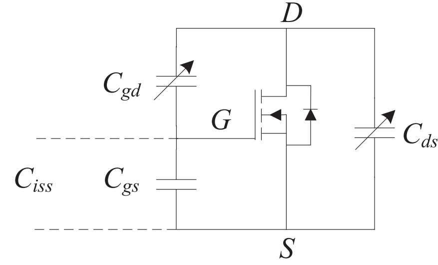

Fig. 4. Parasitic capacitances in SiC MOSFETs.

$$C_{\text{iss}} = C_{\text{gs}} + \frac{C_{\text{gd}}.C_{\text{ds}}}{C_{\text{gd}} + C_{\text{ds}}}. \tag{12}$$

The gate-to-source capacitance remains constant as the gate-to-source voltage varies, originating from the gate-oxide material between the gate metallization and doping material in the source. However, C_{gd} and C_{ds} are the junction capacitance within the device's p–n junction, and their values change based on the applied voltage. Specifically, the junction capacitance decreases as the voltage increases. During switching transients, variations in the dc-link voltage lead to an overall nonlinear change in the input capacitance. As shown in (6) and (7), ($\frac{di_{D,\text{on}}}{dt}$) and ($\frac{di_{D,\text{off}}}{dt}$), are influenced by the nonlinear behavior of C_{iss}. Given this nonlinear relationship, it is advised to perform a one-time calibration before system operation to ensure accurate measurements.

III. Proposed Circuit for Switching Transients Measurement

This section introduces a new circuit to capture switching transients. The proposed circuit utilizes the voltage drop across the common source stray inductance to accurately measure t_r and t_f of the SiC MOSFET. Despite the relatively small value of stray inductance, the voltage drop across the common source is still significant due to the SiC MOSFET's higher rate of change of drain current compared to a Si MOSFET. As a result, the voltage drop becomes easily measurable. This voltage is specifically generated during switching transients, and it is observed that the spikes in the common source voltage have a duration that aligns with the switching transients. Also, it is demonstrated that modifying the gate resistance allows for the adjustment of sensitivity in order to achieve the desired resolution in capturing transient times. The circuit diagram of the proposed circuit for capturing switching transients is depicted in Fig. 5. For conducting the switching transient measurement, initially, a large gate resistance ($R_{g,L}$) is inserted into the gate path for less than a single switching cycle, utilizing auxiliary switches (S_1, S_2). Subsequently, the common source voltage is measured via a high input impedance buffer. The obtained voltage is directed through an *RC* filter to eliminate noise originating from power loop parasitic inductance and prevent erroneous operation of

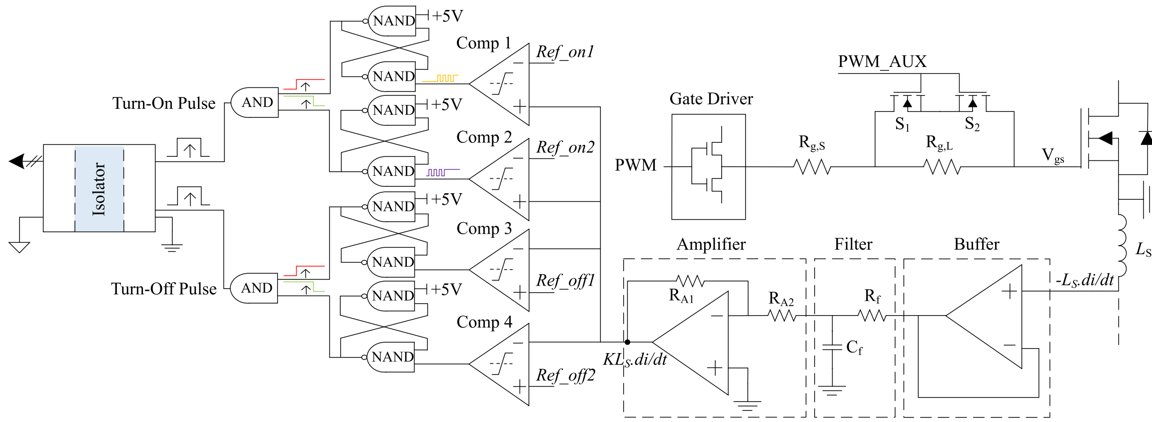

Fig. 5. Circuit diagram of the proposed switching transients measurement circuit.

comparators. The input stage's gain can be obtained by

$$\lim_{j\omega\to\infty} G(j\omega) = \frac{R_{A1}L_S}{R_{A2}R_fC_f}. \tag{13}$$

It should be noted that the careful selection of RC values in (12) is necessary to ensure suitable high-frequency operation. The subsequent step involves inverting and amplifying the signal while considering the input voltage limitations imposed by the comparators. Even in low-current devices, the rate of change of drain current remains sufficiently high to generate measurable common-source stray inductance voltage, even without amplification. However, the amplifier stage can fine-tune this voltage. The reference values of the comparators are carefully selected to accurately capture the initial ramp of the common source voltage during both turn-ON and turn-OFF transients. The captured times correspond to a fraction of the overall t_r and t_f. As a result of conducting the measurement under high gate resistance, the captured fraction of t_r and t_f retains the capability to offer highly precise temperature measurements. It is important to emphasize that the insertion of the large gate resistance occurs only for a brief duration of less than one switching cycle. Following this, the circuit promptly returns to its regular operation until the next interrupt flag is received from the microcontroller for measurement. Importantly, this brief interruption does not have any adverse impact on the normal operation of the converter. The output signals from the comparators are fed into an set-reset flip-flop (SR) flip-flop logic circuit, which includes two NAND gates, serving the purpose of noise elimination and preventing false triggering during the rising and falling edges. The flip-flops respond to the initial edge and are reset after each measurement takes place. The output from the flip-flop logic is directed to an AND logic circuit, which generates a pulse with a width corresponding to the duration of the switching transients. Although the common source voltage can be measured using the microcontroller's ADC, the proposed voltage conversion method transforms this voltage into pulses with a specific width. The time duration of these pulses can be accurately measured using the C2000 microcontroller's high-resolution capture (HR-Cap) module, which provides a resolution of 300 ps. The proposed circuit is regarded as a comprehensive signal chain and offers a cost-effective solution that can be seamlessly integrated into gate driver ICs.

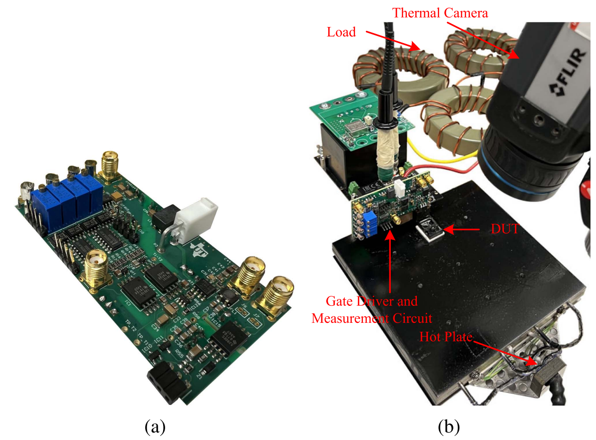

Fig. 6. Photograph of the test setups. (a) Switching transients measurement daughter board. (b) Test setup for junction temperature measurement.

When implementing this method on a separate daughter board, it is recommended to apply the same printed circuit board (PCB) techniques used in the gate driver board designing. Crucially, maintaining a reasonable distance between digital ground and power ground is essential to prevent noise interference on comparators.

To validate the accuracy of the proposed circuit, a custom-designed setup is utilized, offering the flexibility to be configured as either double pulse or buck circuits. The experimental setup is presented in Fig. 6. The test setup incorporates an inductor with a size of 650 μH, an output capacitor of 180 μF, and a switching frequency of 200 kHz in buck mode. Similar to other TSEP-based methods used for junction temperature measurement, this circuit requires an initial calibration during system start-up. However, what sets this circuit apart is its ability to compensate for the aging effect, eliminating the need for periodic recalibration like other TSEP-based methods, as further discussed in Section IV.

Fig. 7 displays the experimental waveforms obtained for the drain current, gate–source voltage, as well as the filtered and

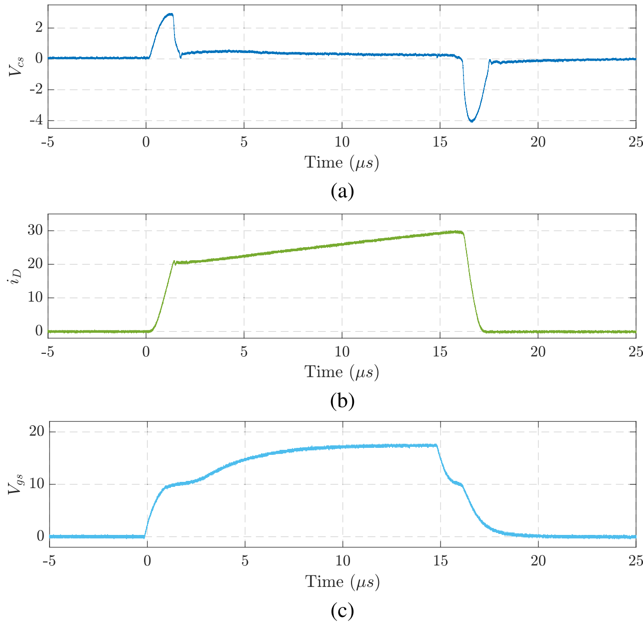

Fig. 7. Experimental waveforms of the switching transients measurement board (V_{ds} = 200 V and $R_g = 1005\,\Omega$). (a) Common source voltage drop. (b) Drain current. (c) Gate–source voltage.

inverted common source voltage (V_{cs}). In real applications, the dc-bus voltage remains constant, and therefore, for these experiments, it is set to 200 V. The circuit is operated using a gate resistance of 5 Ω, and a 1 KΩ resistance is inserted to capture the switching transients. As observed, V_{sc} during turn-ON and turn-OFF transients is approximately 3 V and 4 V, respectively. This voltage level is reasonably significant, making it suitable for capturing and measuring. Fig. 8 illustrates the pulses representing t_r and t_f. In this case, the comparator references are selected to capture the initial ramp in the switching transients. This ensures a strong linear correlation between the transient pulses and the junction temperature.

Fig. 9 exhibits the turn-ON transient pulse at various junction temperatures. The V_{sc} references are set at 0.5 V and 2.5 V to generate the rising edge and falling edge signals, respectively. To verify the precision of the proposed circuit, the SiC MOSFET is decapsulated within the die area and directly monitored using an Infrared (IR) camera. In order to enhance the IR radiation emissivity, the decapsulated area is coated with black paint and a layer of silicone conformal coating. This coating serves multiple purposes, including preventing electrical leakage, short circuits, and unintended electrical connections by providing insulation between conductive wires. In addition, it acts as a protective barrier against moisture, dust, and other environmental factors. Fig. 10 presents the accuracy verification of the junction temperature measurement circuit through direct monitoring of the die temperature using an IR camera. The MOSFET chip area is partially decapsulated to avoid damaging bond wires. An IR camera directly measures the actual junction temperature. The chip area is painted black to enhance IR radiation emissivity. Subsequently, the chip area is covered by silicone conformal

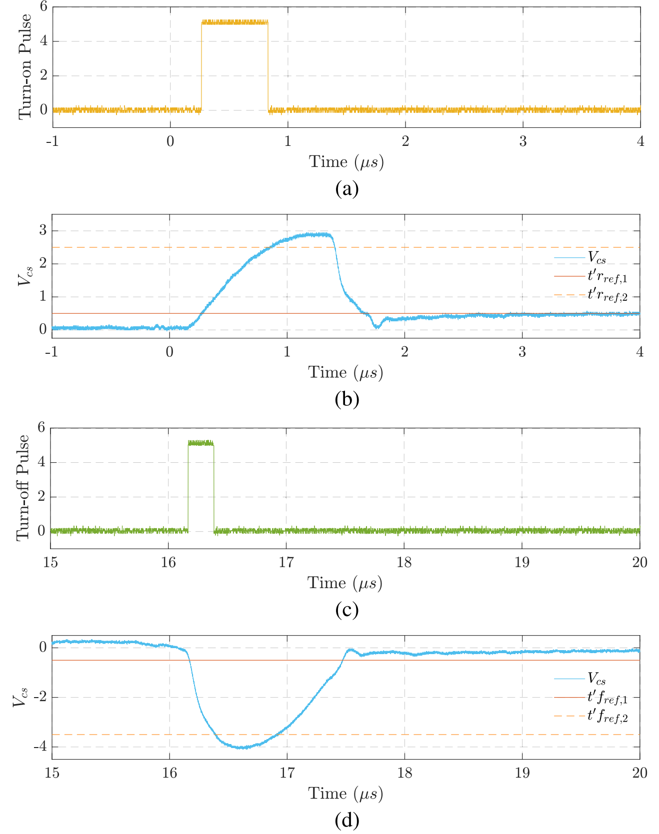

Fig. 8. Experimental waveforms of the logic output (V_{ds} = 200 V and R_g = 1005 Ω). (a) t'_r pulse. (b) Common source voltage during turn-ON transient and t'_r reference values ($t'r_{\mathrm{ref},1}$ = 0.5 V and $t'r_{\mathrm{ref},2}$ = 2.5 V). (c) t'_f pulse. (d) Common source voltage during turn-OFF transient and t'_f reference values ($t'f_{\mathrm{ref},3} = -0.5$ V and $t'f_{\mathrm{ref},4} = -3.5$ V).

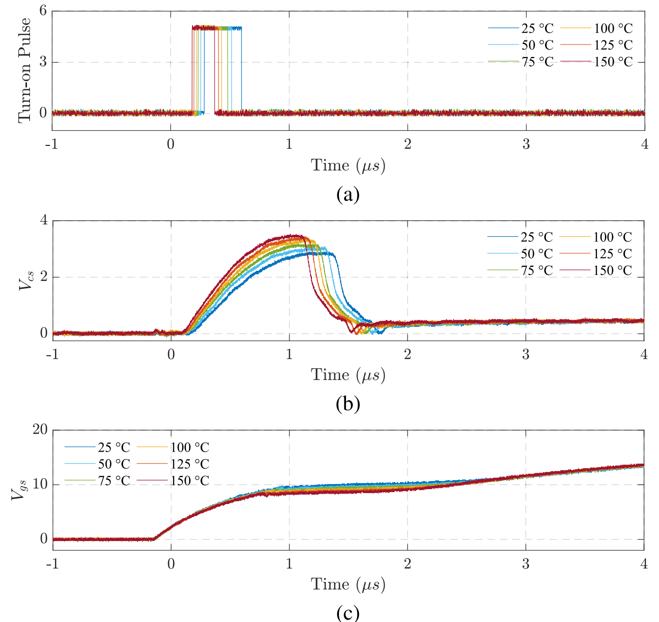

Fig. 9. Experimental waveforms of t'_r measurement at different junction temperatures. (a) t'_r pulse. (b) Common source voltage during turn-ON transient. (c) Gate–source voltage.

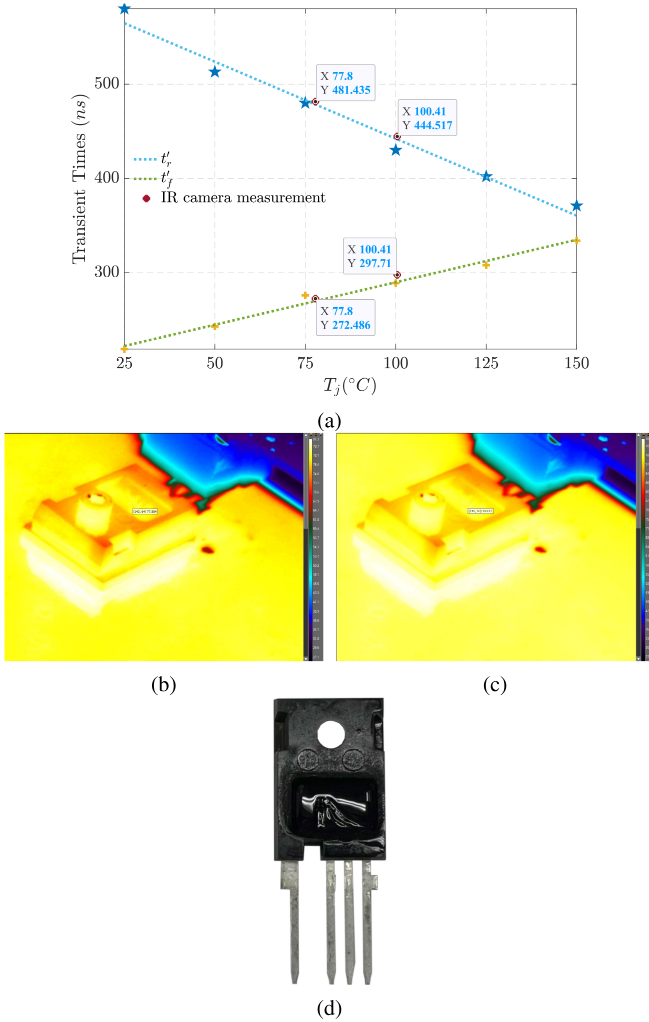

Fig. 10. Accuracy verification of junction temperature measurement circuit using direct die temperature monitoring with the IR camera. (a) Verification of junction temperature measurement at two operating points. (b) IR camera results at a steady state of 77.80 °C. (c) IR camera results at a steady state of 100.41 °C. (d) Decapsulated, silicone conformal-coated, black-painted SiC MOSFET to validate junction temperature using an IR camera.

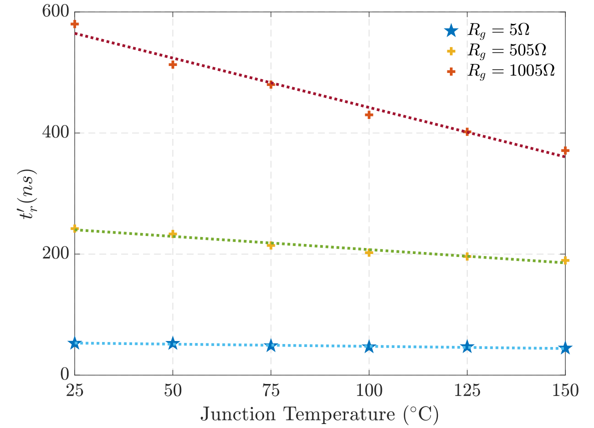

Fig. 11. t_r' versus junction temperature at different external gate resistances ($V_{\text{ds}} = 200$ V and $I_D = 20$ A).

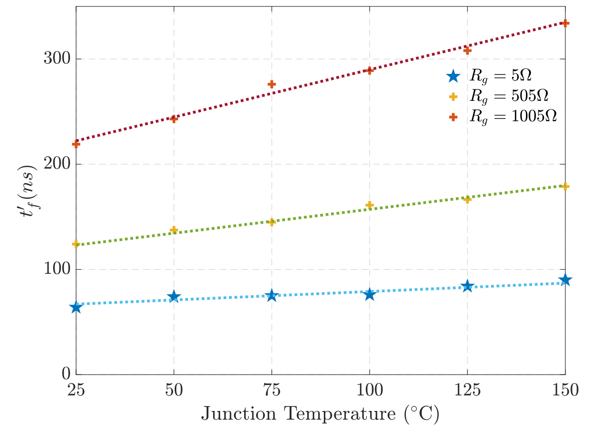

Fig. 12. t_f' versus junction temperature at different external gate resistances ($V_{\text{ds}} = 200$ V and $I_D = 20$ A).

TABLE I
LINEAR FORECAST PARAMETERS FOR t_r' AND t_f' VERSUS JUNCTION TEMPERATURE AT DIFFERENT GATE RESISTANCES

R_g	t_r' slope	t_r' value at 25° C	t_f' slope	t_f' value at 25° C
5 Ω	−72 ps/° C	53 ns	4 ps/° C	67 ns
505 Ω	−436.8 ps/° C	240.1 ns	453.6 ps/° C	123.1 ns
1005 Ω	−873.6 ps/° C	580.9 ns	860.8 ps/° C	222.2 ns

coating to protect it from high electrical fields and static discharge. The measured temperature is then compared with the temperature obtained from the pulse width measurement. Given that t_r' and t_f' vary approximately by 1.67 ns and 0.89 ns per degree, respectively, and taking into account the 300 ps resolution of the microcontroller's HR-Cap module, the circuit can measure the temperature with an error of less than 1 °C.

Figs. 11 and 12 illustrate the correlation between t_r' and t_f' and junction temperature under various external gate resistances. It is important to highlight that although the circuit can successfully capture switching transients with a low gate resistance, the insertion of a higher resistance is essential. This higher resistance enables significant observation of temperature-dependency and aging-dependency in the switching transients. Table I presents a summary of the linear regression parameters for t_r' and t_f' in relation to junction temperature under various gate resistances.

While both t_r' and t_f' can be utilized for junction temperature measurement, it is observed that t_r' exhibits higher sensitivity and is deemed more suitable for this purpose. Furthermore, the insertion of a large gate resistance prior to the turn-ON transient is a more straightforward approach. For junction temperature monitoring, it is recommended to perform online measurement of t_r'. Periodically, the measurement of t_f' can be conducted to recalibrate the temperature dependency lookup table for t_r', which will be discussed in the subsequent section. It is important to note that the measurement of t_f' can be performed in situ during system start-up.

In order to verify the efficacy of the proposed method during actual converter operation, the test setup is configured as a

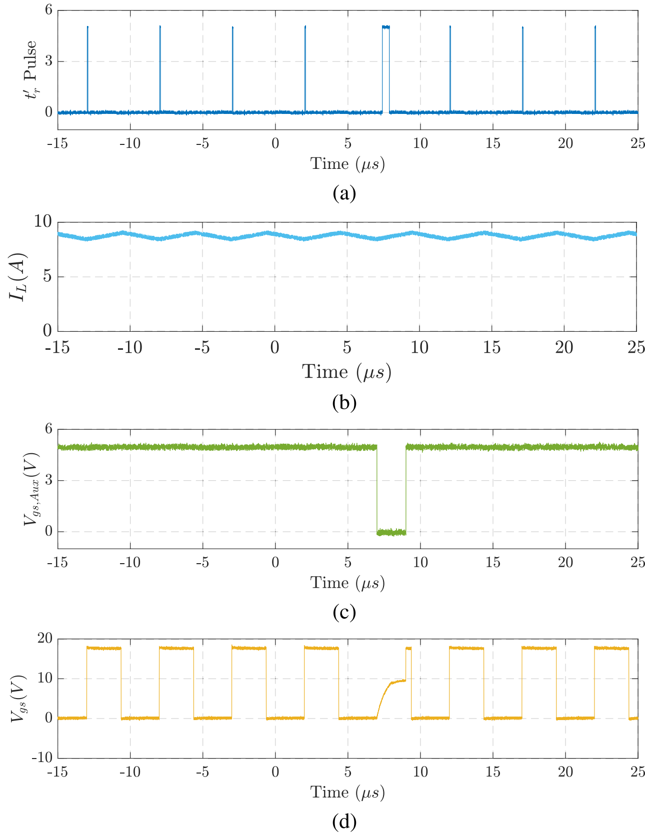

Fig. 13. Experimental waveforms of the switching transients measurement board at converter continuous operation ($V_{\mathrm{ds}} = 200$ V). (a) t'_r pulse. (b) Drain current ($f_{\mathrm{sw}} = 40$ kHz). (c) Gate–source voltage of auxiliary switches (S_1 and S_2). (d) Gate–source voltage.

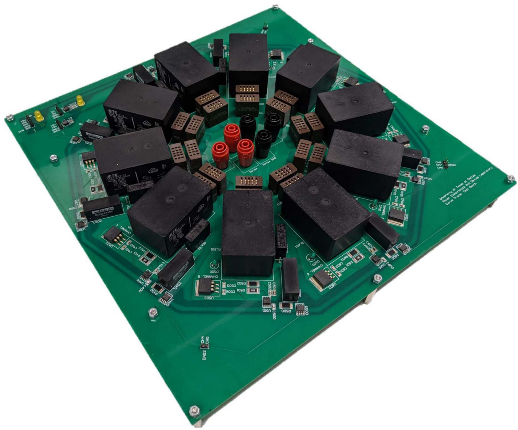

Fig. 14. Photograph of the ACGB test setups.

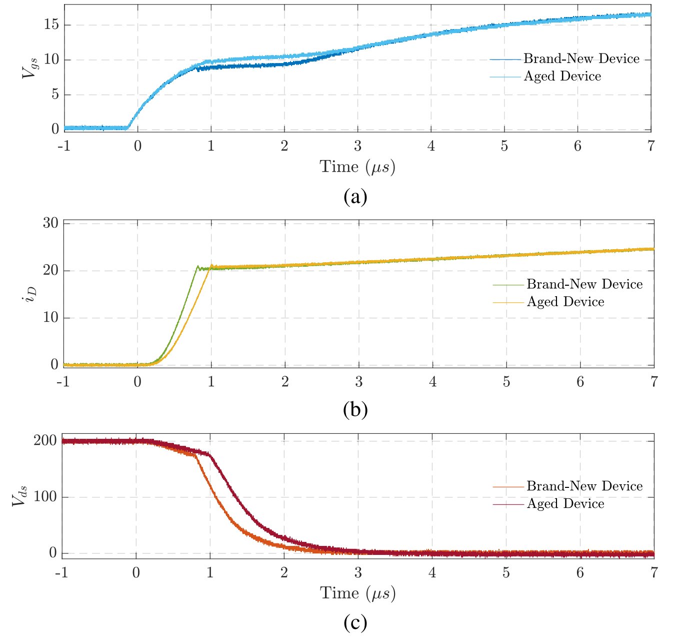

Fig. 15. Aging effect on turn-ON switching transient for SiC MOSFET during ACGB test ($R_g = 1005\,\Omega$). (a) Gate–source voltage. (b) Drain current. (c) Drain–source voltage.

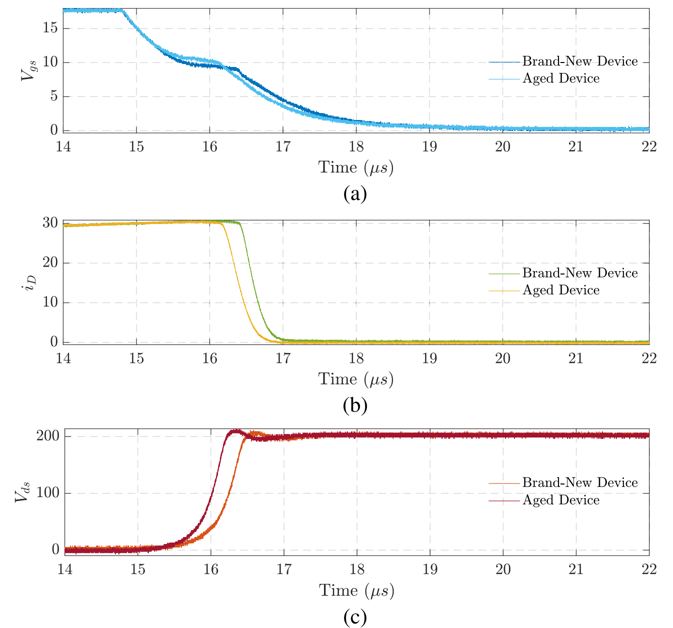

Fig. 16. Aging effect on turn-OFF switching transient for SiC MOSFET during ACGB test ($R_g = 1005\,\Omega$). (a) Gate–source voltage. (b) Drain current. (c) Drain–source voltage.

buck converter. The large resistance is inserted by the auxiliary switches for a duration of $2\,\mu$s under the control of the microcontroller. After the measurement is completed, the system immediately returns to normal operation. Fig. 13 displays the experimental waveforms captured by the switching transients measurement board during continuous operation of the converter, with V_{ds} maintained at 200 V.

In commercial microcontrollers, the HR-Cap module offers a resolution of 300 ps. This capability allows the proposed circuit to accurately measure temperature, even when utilizing a relatively small resistance. Furthermore, the converter operation remains unaffected by the use of a large resistance, enabling proposed circuit to confidently achieve high-resolution temperature measurements with a 1 KΩ resistance insertion.

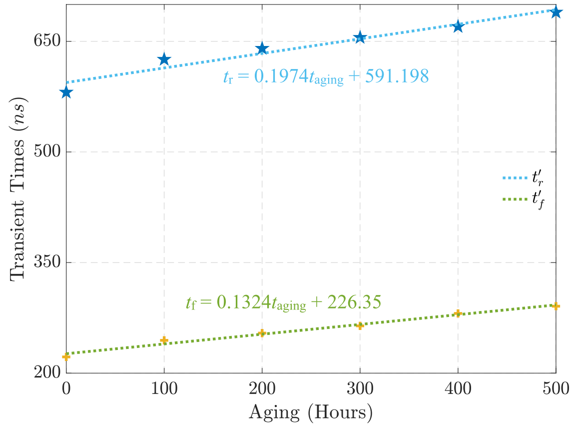

Fig. 17. t'_r and t'_f versus aging hours during ACGB test ($t_j = 25\,°$C, $R_g =$ 1005 Ω, and $V_{\mathrm{ds}} = 200$ V).

TABLE II
CORRELATION BETWEEN t'_r AND t'_f WITH DIFFERENT OPERATING CONDITIONS

Operation conditions	t'_r	t'_f
Temperature	Negative	Positive
Gate oxide degradation	Positive	Positive
Gate resistance	Positive	Positive
DC bus voltage	Negative	Positive

IV. AGING EFFECT COMPENSATION

The literature presents various temperature measurement methods based on TSEPs. However, it is important to note that TSEP methods are generally susceptible to aging effects. This implies that all TSEP-based methods require periodic calibration throughout their lifespan, posing challenges for practical applications. This article employs the measurement of switching transient times during turn-ON and turn-OFF events to estimate the junction temperature, incorporating aging compensation technique. Table II presents the relationship between t'_r and t'_f under various operating conditions. For SiC MOSFETs, it is observed that turn-ON and turn-OFF switching transient times exhibit negative and positive temperature dependencies, respectively. Based on the experimental results shown in Figs. 10, 11, and 16, t'_r and t'_f can be represented using a linear relationship that considers both aging and temperature, along with an offset. As a result, we can describe the t'_r and t'_f as follows:

$$\begin{cases} t'_r = -ET_j + FA_g + K_{\mathrm{on}} \\ t'_f = GT_j + HA_g + K_{\mathrm{off}} \end{cases} \tag{14}$$

$$A_g = K_1 t'_r + K_2 t'_f + K_3 \tag{15}$$

where E, F, G, and H are positive constants. In practical applications, the gate resistance and dc-bus voltage remain constant, and their impact can be incorporated into the one-time calibration process. Among the three primary failure mechanisms in SiC MOSFETs, namely package degradation, gate oxide degradation, and body diode degradation, it is worth noting that only gate oxide degradation has the potential to impact the parameters associated with switching transient times. A set of ten SiC MOSFETs with a blocking voltage of 1.2 KV and an on-resistance of 80 mΩ were subjected to an ACGB test to induce aging. Fig. 14 depicts the setup used for the ACGB test. In this test, the device under test operates at a constant current while applying high gate bias at elevated temperatures. The selected channel current is adjusted to achieve a junction temperature of 150 °C, and a positive gate bias is applied to generate an electric field across the gate oxide. The gate–source voltage for this test is set to 30 V, and considering the gate oxide thickness of the tested SiC MOSFET (40 nm), the electric field across the gate oxide reaches 7 MV/cm. The gate leakage current is continuously monitored through the gate resistance using a differential amplifier. If the gate leakage current exceeds 1 mA, the test is halted.

Figs. 15 and 16 illustrate the impact of aging on the turn-ON and turn-OFF switching transients of the SiC MOSFET during the ACGB test, respectively. The aging mechanisms have a noticeable impact on the gate plateau, delay times, and transient times, thereby emphasizing the importance of implementing aging compensation mechanisms. Fig. 17 presents the relationship between t'_r and t'_f and aging hours during the ACGB test. The aging data can be used to program a fitted curve for the purpose of aging compensation.

The proposed method necessitates calibration prior to system operation to ensure precise measurements. This calibration challenge is common in monitoring methods based on electrical parameters and warrants further investigation in future research.

V. CONCLUSION

This article proposes a new circuit design that offers an aging-compensated method to measure the junction temperature of SiC MOSFETs by leveraging the switching transients. The circuit utilizes the voltage drop across the common source stray inductance to measure part of the switching transients at the t_r and t_f. The proposed circuit captures the duration of the switching transients and converts them into pulse widths. These pulse widths can be accurately measured using an HR-Cap module in a microcontroller. The experimental results validate the accuracy of the proposed circuit, with a high correlation between the measured pulses and the junction temperature of the SiC MOSFET. This measurement technique offers a cost-effective solution that can be integrated into gate driver ICs. Also, the proposed circuit addresses the limitations of existing temperature measurement methods based on thermal-sensitive electrical parameters by eliminating the need for frequent recalibration. The circuit compensates for the aging dependencies of the t_r and t_f at the switching transients. It is shown that the measurement of the t_r is particularly suitable for temperature monitoring, and periodic measurement of the fall time can be used to recalibrate the temperature dependency lookup table.

In this research, the SiC MOSFET undergoes decapsulation, allowing for direct monitoring using an IR camera. Through experimental results, the precision and reliability of the proposed circuit are demonstrated, showcasing temperature measurement

errors of less than 1 °C. The circuit can be seamlessly integrated into practical converter systems, and its interruption during measurement does not affect the normal operation of the converter. By accurately capturing the switching transients and estimating the junction temperature, the proposed circuit enables effective thermal management and protection of SiC MOSFETs.

REFERENCES

[1] B. J. Baliga, *Fundamentals of Power Semiconductor Devices*. Berlin, Germany: Springer, 2010.

[2] K. Suganuma, *Wide Bandgap Power Semiconductor Packaging: Materials, Components, and Reliability (Electronic and Optical Materials)*. Sawston, U.K.: Woodhead Publishing, 2018.

[3] K. Boomer, J.-M. Lauenstein, and A. Hammoud, “Body of knowledge for silicon carbide power electronics,” 2016. [Online]. Available: https://ntrs.nasa.gov/archive/nasa/casi.ntrs.nasa.gov/20170003922.pdf

[4] C. Li, H. Luo, C. Li, W. Li, H. Yang, and X. He, “Online junction temperature extraction of SiC power MOSFETs with temperature sensitive optic parameter (TSOP) approach,” *IEEE Trans. Power Electron.*, vol. 34, no. 10, pp. 10143–10152, Oct. 2019.

[5] G. Breglio, A. Irace, P. Spirito, R. Letor, and S. Russo, “Fast transient infrared thermal analysis of smart power MOSFETS in permanent short circuit operation,” in *Proc. IEEE Int. Symp. Power Semicond. Devices IC’s*, 2006, pp. 1–4.

[6] A. S. Bahman, K. Ma, P. Ghimire, F. Iannuzzo, and F. Blaabjerg, “A 3-D-Lumped thermal network model for long-term load profiles analysis in high-power IGBT modules,” *IEEE Trans. Emerg. Sel. Topics Power Electron.*, vol. 4, no. 3, pp. 1050–1063, Sep. 2016.

[7] K. Ma, N. He, M. Liserre, and F. Blaabjerg, “Frequency-domain thermal modeling and characterization of power semiconductor devices,” *IEEE Trans. Power Electron.*, vol. 31, no. 10, pp. 7183–7193, Oct. 2016.

[8] R. Sajadi et al., “Third quadrant operation of SiC MOSFETs: Comprehensive analysis and condition monitoring solution,” *IEEE Trans. Compon., Packag. Manuf. Technol.*, vol. 14, no. 5, pp. 851–861, May 2024, doi: 10.1109/TCPMT.2024.3385312.

[9] R. Sajadi, C. Xu, B. T. Vankayalapati, M. Farhadi, and B. Akin, “Reliability evaluation of isolated LDMOS devices and condition monitoring solution,” *IEEE Trans. Compon., Packag. Manuf. Technol.*, vol. 14, no. 5, pp. 841–850, May 2024, doi: 10.1109/TCPMT.2024.3385310.

[10] H. Luo, W. Li, F. Iannuzzo, X. He, and F. Blaabjerg, “Enabling junction temperature estimation via collector-side thermo-sensitive electrical parameters through emitter stray inductance in high-power IGBT modules,” *IEEE Trans. Ind. Electron.*, vol. 65, no. 6, pp. 4724–4738, Jun. 2018.

[11] M. Farhadi, B. T. Vankayalapati, R. Sajadi, and B. Akin, “AC power cycling test setup and condition monitoring tools for SiC-based traction inverters,” *IEEE Trans. Veh. Technol.*, vol. 72, no. 10, pp. 12728–12743, Oct. 2023.

[12] B. T. Vankayalapati, M. Farhadi, R. Sajadi, B. Akin, and H. Tan, “A practical switch condition monitoring solution for sic traction inverters,” *IEEE Trans. Emerg. Sel. Topics Power Electron.*, vol. 11, no. 2, pp. 2190–2202, Apr. 2023.

[13] H. Niu and R. D. Lorenz, “Sensing power MOSFET junction temperature using circuit output current ringing decay,” in *Proc. IEEE Energy Convers. Congr. Expo.*, 2013, pp. 4270–4277.

[14] M. Farhadi, B. T. Vankayalapati, and B. Akin, “Reliability evaluation of SiC MOSFETs under realistic power cycling tests,” *IEEE Power Electron. Mag.*, vol. 10, no. 2, pp. 49–56, Jun. 2023.

[15] L. Cheng, A. K. Agarwal, S. Dhar, S.-H. Ryu, and J. W. Palmour, “Static performance of 20 A., 1200 V. 4H-SiC power MOSFETs at temperatures of -187 C. to 300 C,” *J. Electron. Mater.*, vol. 41, pp. 910–914, 2012.

[16] A. Griffo, J. Wang, K. Colombage, and T. Kamel, “Real-time measurement of temperature sensitive electrical parameters in SiC power MOSFETs,” *IEEE Trans. Ind. Electron.*, vol. 65, no. 3, pp. 2663–2671, Mar. 2018.

[17] H. Niu and R. D. Lorenz, “Sensing power MOSFET junction temperature using gate drive turn-on current transient properties,” in *Proc. IEEE Energy Convers. Congr. Expo.*, 2014, pp. 2909–2916.

[18] N. Baker, S. Munk-Nielsen, F. Iannuzzo, and M. Liserre, “Online junction temperature measurement using peak gate current,” in *Proc. IEEE Appl. Power Electron. Conf. Expo.*, 2015, pp. 1270–1275.

[19] R. Wang, J. Sabate, K. Mainali, T. Sadilek, P. Losee, and Y. Singh, “SiC device junction temperature online monitoring,” in *Proc. IEEE Energy Convers. Congr. Expo.*, 2018, pp. 387–392.

[20] F. Yang, S. Pu, C. Xu, and B. Akin, “Turn-on delay based real-time junction temperature measurement for SiC MOSFETs with aging compensation,” *IEEE Trans. Power Electron.*, vol. 36, no. 2, pp. 1280–1294, Feb. 2021.

[21] Z. Zhang et al., “Online junction temperature monitoring using intelligent gate drive for SiC power devices,” *IEEE Trans. Power Electron.*, vol. 34, no. 8, pp. 7922–7932, Aug. 2019.

[22] E. Hashemzadeh, M. Aghamohammadi, M. Asadi, J. Z. Moghaddam, and J. M. Guerrero, “Secondary control for a D-Statcom DC-link voltage under capacitance degradation,” *IEEE Trans. Power Electron.*, vol. 36, no. 11, pp. 13215–13224, Nov. 2021.

[23] F. Yang, E. Ugur, and B. Akin, “Evaluation of aging’s effect on temperature-sensitive electrical parameters in SiC MOSFETs,” *IEEE Trans. Power Electron.*, vol. 35, no. 6, pp. 6315–6331, Jun. 2020.

[24] P. Sun, C. Gong, X. Du, Q. Luo, H. Wang, and L. Zhou, “Online condition monitoring for both IGBT module and DC-Link capacitor of power converter based on short-circuit current simultaneously,” *IEEE Trans. Ind. Electron.*, vol. 64, no. 5, pp. 3662–3671, May 2017.

[25] M. Du, J. Xin, H. Wang, Z. Ouyang, and K. Wei, “Estimating junction temperature of SiC MOSFET using its drain current during turn-on transient,” *IEEE Trans. Electron Devices*, vol. 67, no. 5, pp. 1911–1918, May 2020.

[26] P. Sun et al., “An online junction temperature monitoring correction method for SiC MOSFETs at different parasitic parameters,” *IEEE Trans. Emerg. Sel. Topics Power Electron.*, vol. 10, no. 5, pp. 5007–5018, Oct. 2022.

[27] X. Meng, M. Zhang, S. Feng, Y. Tang, and Y. Zhang, “Online temperature measurement method for SiC MOSFET device based on gate pulse,” *IEEE Trans. Power Electron.*, vol. 39, no. 4, pp. 4714–4724, Apr. 2024.

[28] Y. Yang and P. Zhang, “In situ junction temperature monitoring and bond wire detecting method based on IGBT and FWD on-state voltage drops,” *IEEE Trans. Ind. Appl.*, vol. 58, no. 1, pp. 576–587, Jan./Feb. 2022.

[29] T. Tang, W. Song, K. Yang, and J. Chen, “A junction temperature online monitoring method for IGBTs based on turn-off delay time,” *IEEE Trans. Ind. Appl.*, vol. 59, no. 5, pp. 6399–6411, Sep./Oct. 2023.

[30] H. Li, X. Liao, Y. Hu, Z. Zeng, E. Song, and H. Xiao, “Analysis of SiC MOSFET di/dt and its temperature dependence,” *IET Power Electron.*, vol. 11, no. 3, pp. 491–500, 2018.

[31] M. Hasanuzzaman, S. K. Islam, L. M. Tolbert, and M. T. Alam, “Temperature dependency of MOSFET device characteristics in 4H-and 6H-Silicon carbide (SiC),” *Solid-State Electron.*, vol. 48, no. 10/11, pp. 1877–1881, 2004.

[32] J. Gonzalez, O. Alatise, J. Hu, L. Ran, and P. A. Mawby, “An investigation of temperature-sensitive electrical parameters for SiC power MOSFETs,” *IEEE Trans. Power Electron.*, vol. 32, no. 10, pp. 7954–7966, Oct. 2017.

[33] M. Farhadi, F. Yang, S. Pu, B. T. Vankayalapati, and B. Akin, “Temperature-independent gate-oxide degradation monitoring of SiC MOSFETs based on junction capacitances,” *IEEE Trans. Power Electron.*, vol. 36, no. 7, pp. 8308–8324, Jul. 2021.

[34] I. Filanovsky and A. Allam, “Mutual compensation of mobility and threshold voltage temperature effects with applications in CMOS circuits,” *IEEE Trans. Circuits Syst. I: Fundam. Theory Appl.*, vol. 48, no. 7, pp. 876–884, Jul. 2001.

Masoud Farhadi (Member, IEEE) received the B.Sc. degree (Hons.) in electrical engineering and the M.Sc. degree (Hons.) in power engineering (power electronics and systems) from the Department of Electrical Engineering, University of Tabriz, Tabriz, Iran, in 2013 and 2016, respectively, and the Ph.D. degree in electrical engineering from The University of Texas at Dallas, Richardson, TX, USA, in 2023.

He is currently a Systems Engineer with Texas Instruments Incorporated, Dallas, TX, USA. His current research interests include analysis and control of power electronic converters, reliability of power electronic systems, wide bandgap semiconductor device reliability, and renewable energy conversion systems.

Mr. Farhadi was the recipient of the 2020 Jonsson School Industrial Advisory Council Fellowship, 2021 OK Kyun Kim and Youngmoo Cho Kim Graduate Fellowship and 2022, 2023 Excellence in Education Doctoral Fellowship from the University of Texas at Dallas. He is also the recipient of the Doctoral Dissertation Excellence Award 2023 from the University of Texas at Dallas.

Rahman Sajadi received the B.Sc. degree in electrical engineering from Bu-Ali Sina University, Hamedan, Iran, in 2014, and the M.Sc. degree in electrical engineering from the University of Tehran, Tehran, Iran, in 2016. He is currently working toward the Ph.D. degree in electrical engineering with the University of Texas at Dallas, Richardson, TX, USA.

His research interests include design, modeling, reliability and control of power converters, wide bandgap semiconductor reliability, multilevel converters, and renewable energy systems.

Bhanu Teja Vankayalapati (Member, IEEE) received the B.Tech. degree in electrical engineering and the M.Tech. degree in power electronics from the Indian Institute of Technology (BHU), Varanasi, India, in 2017, and the Ph.D. degree in electrical engineering from the University of Texas at Dallas, Richardson, TX, USA, in 2022.

From 2017 to 2018, he was a Project Engineer with the Indian Institute of Technology, Kanpur, India. He is currently an Application Engineer with Texas Instruments Incorporated, Dallas, TX, USA. His research areas include WBG device applications, WBG reliability, converter design, and embedded control.

Bilal Akin (Fellow, IEEE) received the Ph.D. degree in electrical engineering from Texas A&M University, College Station, TX, USA, in 2007.

From 2005 to 2008, he was an R&D Engineer with Toshiba Industrial Division, Houston, TX, USA. From 2008 to 2012, he was an R&D Engineer with C2000 DSP Systems, Texas Instruments Incorporated. Since 2012, he has been with The University of Texas at Dallas, Richardson, TX, USA, as a Faculty. His research interests include design, control and diagnosis of electric motors and drives, digital power control and management, and fault diagnosis and condition monitoring of power electronics components and ac motors.

Dr. Akin was a recipient of NSF CAREER 2015 Award, IEEE IAS Transactions First Place Prize Paper Award and Top Editors Recognition Award from IEEE TVT Society, and two Jonsson School Faculty Research Awards. He is currently an Area Editor of IEEE TRANSACTIONS ON VEHICULAR TECHNOLOGY.